New Constant Electrical Power Soft-Stalling Control for Small-Scale VAWTs

Ashraf Ahmed, *Student Member, IEEE*, Li Ran, *Senior Member, IEEE*, and Jim R. Bumby

***Abstract*—This paper presents a constant power soft-stall control scheme for a vertical-axis wind turbine (VAWT) fitted with a permanent magnet generator. Small-scale VAWTs are attractive due to their ability to capture wind from different directions without using yaw; this simplifies the design and gives the turbine tolerance to turbulence in urban areas. One difficulty with VAWTs is to prevent overspeeding and component overloading at excessive wind velocities. This paper suggests that necessary control can be achieved by controlling the electric power in order to operate the turbine in the stall region. This control strategy attenuates the stress in the system, while smoothing the power generated. It is shown that the controller can stabilize the nonlinear system using an adaptive current feedback loop. The controller does not need wind velocity or turbine speed, but is based on the current and voltage measured on the dc side of the rectifier connected to the permanent magnet synchronous generator. Maximum power point tracking (MPPT) control is provided in normal operation. Simulation and experimental results are presented.**

***Index Terms*—High-wind velocity control, permanent magnet synchronous generator (PMSG), power control, soft stalling, vertical-axis wind turbine (VAWT).**

NOMENCLATURE

e_w	Generator EMF (electromotive force) (V) (referred to dc side of generator rectifier).
v_w	Generator rectifier dc-side voltage (V).
i_w	Generator rectifier dc-side current (A).
K_w	Generator EMF constant (V·s/rad).
C_p	Wind turbine power coefficient.
R_w	Twice of permanent magnet synchronous generator (PMSG) per phase resistance (Ω).
ω_m	Rotor speed (rad/s).
J	Moment of inertia (kg·m^2).
ρ	Air density (kg/m^3).
λ	Tip speed ratio of wind turbine.
v_s	Wind velocity (m/s).
R	Equivalent radius of turbine (m).
T_m	Turbine mechanical torque (N·m).
T_e	Generator electrical torque (N·m).
T_c	Time constant of soft-stalling compensator (s).
v_L	DC-side voltage to grid inverter (V).
A	Swept area of wind turbine (m^2).
d	Duty ratio of dc link boost converter.
a_1, a_2, a_3	Quadratic curve-fitting coefficients of $C_p - \lambda$ relationship.
m_1, m_2, m_3	Quadratic curve-fitting coefficients of the $V_w - I_w$ lookup table, where V_w and I_w are the mean values of the generator rectifier dc-side voltage and current.

Manuscript received October 20, 2009; revised January 7, 2010. The work was supported in part by the Government of Egypt (Desert Research Institute, Cairo, Egypt). Paper no. TEC-00450-2009.

The authors are with the School of Engineering and Computing Sciences, Science Laboratories, Durham University, Durham DH1 3LE, U.K. (e-mail: ashraf.ahmed@durham.ac.uk; li.ran@durham.ac.uk; j.r.bumby@durham.ac.uk).

Color versions of one or more of the figures in this paper are available online at http://ieeexplore.ieee.org.

Digital Object Identifier 10.1109/TEC.2010.2043737

I. INTRODUCTION

WIND is widely regarded as an alternative source for electrical power generation [1], [2]. Small-scale wind turbines, close to the end users of electricity, are becoming popular due to soaring fuel prices and technical progress, which reduces their manufacturing cost. An American Wind Energy Association (AWEA) report indicates that in U.S., small-scale turbines with unit capacity below 10 kW contribute 80 MW of generated power [1]. Year 2008 saw a 78% growth from the previous year, while the growth rate worldwide was at comparable 53%. Sixty three percent of small-scale wind turbines in U.S. are grid connected. In U.K., small-scale turbines of unit capacity less than 1.5 kW were anticipated to generate 20 000 MW·h in 2009, corresponding to a total installation capacity of 10 MW [2]. In 2005, only 8% of such U.K. turbines were grid connected. This increased to 56% in 2008 is due to the introduction of grid codes or guidelines to permit and regulate the connection. Therefore, this study is orientated toward small-scale grid connected wind turbines, but the results can be extended to standalone systems.

Vertical-axis wind turbines (VAWTs) are attractive for applications in the built environment due to their ability to capture wind from different directions without using yaw; this avoids the associated cost of the yaw system [3], [4]. The electrical components that require maintenance are normally positioned on the supporting platform, and a VAWT is also regarded as being quiet. A major problem with a VAWT is the difficulty to embed into the design a stall mechanism at high-wind velocities to prevent overspeeding, excessive power, and overvoltage if a permanent magnet synchronous generator (PMSG) is used. Such machines are favored for their light weight, high-power density, and high efficiency. The PMSG is often directly coupled to the turbine, eliminating the need of a gearbox, and the associated cost and maintenance issues whilst increasing the system reliability [5].

In a large horizontal-axis wind turbine (HAWT), electrical control is usually used for maximum power point tracking

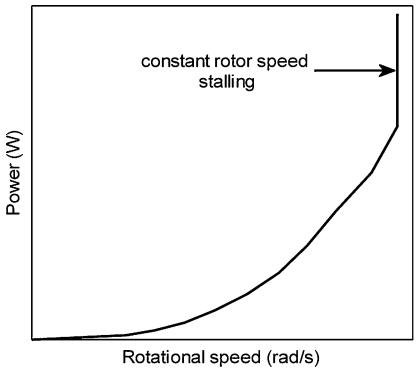

Fig. 1. Power–rotor speed curve in constant speed soft stalling.

(MPPT) and aerodynamic control is used at high-wind velocities to limit the turbine power and rotational speed. Pitching the turbine blades changes the power coefficient (C_p) and constrains the generator current, voltage, and speed [6], [7]. Pitch control increases the system cost and is justifiable for large turbines. A solution in smaller fixed speed turbines is to embed in the blade design a passive stall mechanism, which is activated by high-wind velocities. This can reduce the efficiency, increase the turbine fatigue loading, and reduce the power quality performance; more importantly it will add complexity to a VAWT [8].

Constant speed soft stalling has been proposed for vertical-axis turbines [9], [10] to regulate the rotor speed or the output dc-side voltage of the generator rectifier. This control stalls the turbine and reduces the power captured. Fig. 1 plots the output power against rotor speed in such a scheme; MPPT is normally applied at wind speeds below rated, while at high-wind velocities the rotor speed is kept constant. A problem with this is that the power output is still greater than the rated power, although lower than what would have been if MPPT control had continued to be used at the increased wind velocity. The generator and power electronics must be rated accordingly. Another scheme of electrical control is to connect a mechanically switched three-phase resistor bank at the generator terminal [11], [12]. This induces cost and can reduce generator lifetime as uncontrolled current pulses are drawn. The scheme proposed in this paper aims to stall the turbine at high-wind velocities by keeping the power at the rated value while reducing the speed. This can reduce the cost and improve the quality of the power generated. This require to identify the target operating point, which changes with wind velocity and stabilize the system at that point.

Some algorithms have been proposed to track the wind velocity, which could be used for the purpose of this study. These include hill climbing, which searches the operating point using "perturb and observe" [13] and fuzzy logic [14]. Although such schemes are independent of the generator characteristics, preliminary tests show that these methods are likely to fail to track fast-changing turbulent wind. A more complex method is to estimate the wind velocity using measured generator current and voltage, but needs complex calculation and an accurate system model [15]. The wind velocity can also be estimated using a neural network trained offline, with the rotational speed and power as the inputs [16], [17]. The method depends on training data from a specific site and can be expensive for small turbines. Short-term wind prediction can be performed using an autoregressive statistical model, where a time frame of the energy captured in the past is used to predict future wind velocity [18]. This is statistical and there will be an error in the result. Furthermore, complex computation increases the execution time. Another drawback is again that it is for a particular site and may not be justifiable for small turbines.

The intended contribution of this paper is to demonstrate that the difficulty of identifying the target operating point can be resolved by reversing the normal power-tracking control algorithm. An encoderless scheme is developed in which the rotor speed is measured via the dc-side voltage of the generator rectifier while the power is measured via the dc-side current [19], [20]. The proposed control scheme is set to regulate the speed according to the measured current. For reasons that will become clear in the paper, this will naturally drive the turbine into the stall mode as soon as the wind velocity exceeds the range for maximum power tracking. The total power is kept at the rated value with increased current drawn from the machine, but at a reduced voltage and speed. The stability issue is addressed in the study for a typical vertical-axis turbine while the impact of turbine characteristics, such as solidity, is discussed.

Section II outlines the general concept of the proposed control scheme, which is then designed in Section III. Part of Section III is dedicated to the stability of the controller in the stall mode. Simulation results are presented in Section IV. Experimental validation is provided in Section V.

II. Constant Power Soft-Stalling Concept

The system configuration is shown in Fig. 2, where the PMSG is represented as a three-phase Thévenin equivalent feeding into a diode bridge rectifier. The dc–dc converter controls the power extracted from the generator, while the grid inverter maintains power balance to keep the voltage across the capacitor $C_{\rm dc}$ constant. The control blocks will be expanded on later.

A fixed pitch turbine with a $C_p - \lambda$ curve as shown in Fig. 3(a) should normally operate near the maximum efficiency point ($C_{p\max}$) by adjusting the speed to maintain the tip speed ratio at its optimum value, defined here as $\lambda_{\max}$. If this control is continued at excessive wind velocities, the electrical power, speed, and voltage will exceed the rating of the generator and converter. The control method proposed is to limit the output power and rotor speed by forcing the turbine into the low-speed stall region. To do this, the generator output is temporarily increased by the dc–dc converter to force the turbine to stall. Note that the power coefficient is a function of the tip speed ratio, which subsequently depends on the rotor speed. A wind turbine can either increase or decrease its speed to reduce the power capture by adopting a lowered C_p value. Fig. 3(b) shows the proposed control to decrease the speed, which further prevents the overvoltage problem. As the wind velocity increases from the cut-in value the rotor speed initially increases for maximum power tracking. Beyond this region, say >12 m/s wind velocity, power will be kept constant at the rated value.

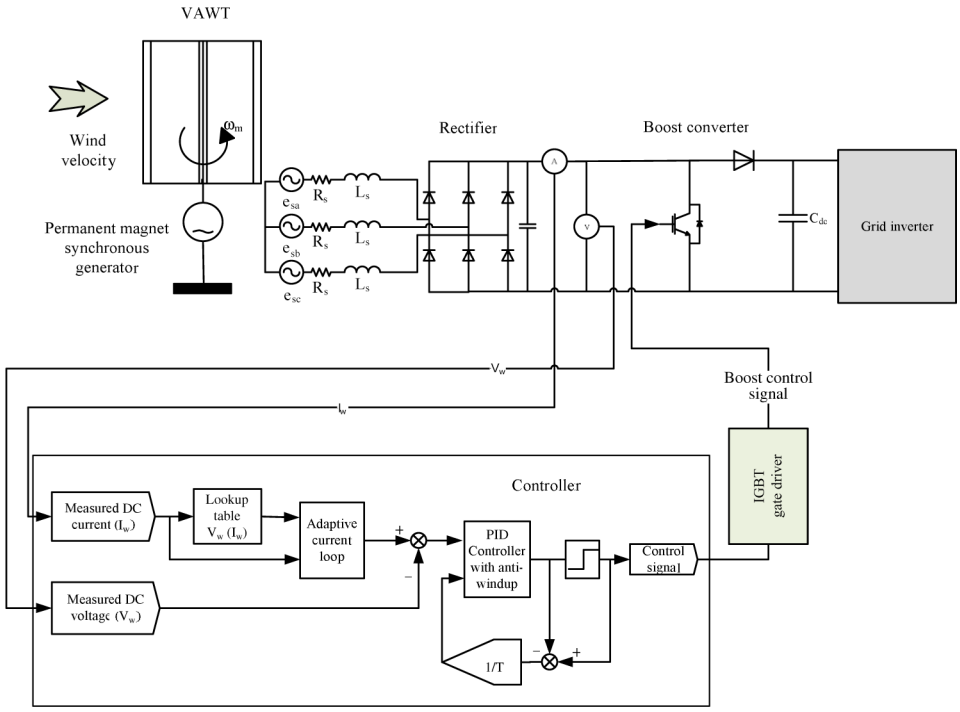

Fig. 2. Block diagram—wind turbine with PMSG and grid connection.

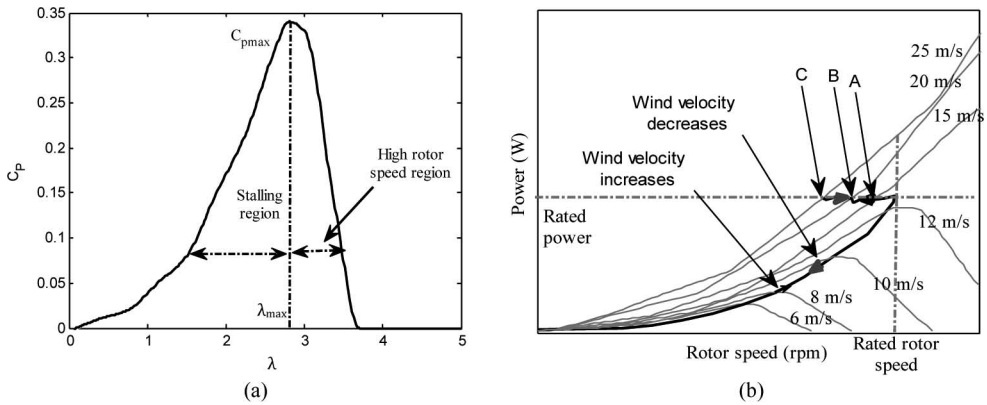

Fig. 3. Concept of constant power soft-stalling control.

The intended operating points are A, B, and C for wind velocities 15, 20, and 25 m/s, respectively. If the wind velocity later reduces to the region for maximum power tracking, the controller should detect this and return to the MPPT mode. The operating point A, B, or C is not explicitly obtainable if the wind velocity is unknown. With a PMSG, the dc-side voltage of the machine rectifier is proportional to the rotor speed. Given the dc-side voltage, power is proportional to the current on the dc side of the rectifier. Based on this, the proposed control is to first establish a lookup table, where the rectifier dc-side current is measured to determine the target dc-side voltage (hence, speed), as shown in Fig. 4. The power tracking control and stalling control then are both reduced to dc-side voltage or speed control, where the control demand is set according to the measured dc-side current. As the wind velocity increases the power initially increases and so does the current. For instance at point "a," the controller will measure the dc-side current i_a and adjust the generator speed so that the dc-side voltage reaches v_a for optimum power extraction. As the wind velocity continues to increase, the dc-side voltage and current increase to the values corresponding to point "b," where the rated condition is reached. Any further increase of the measured dc-side current will require stalling to enforce a reduced turbine speed, and hence, dc-side voltage. If the controller continued to work with MPPT, the generator would follow curve (b–c$''$), which is continuation of "o–a–b," while with constant speed control the system will follow curve (b–c$'$). Using constant power stalling, the system is forced into curve (b–c), where the turbine speed can be decreased by temporarily increasing the electrical power extracted from the generator. The control strategy outlined here for stalling the turbine is indeed the reverse of what is normally used for MPPT. It is clear that by reversing the dc-side voltage

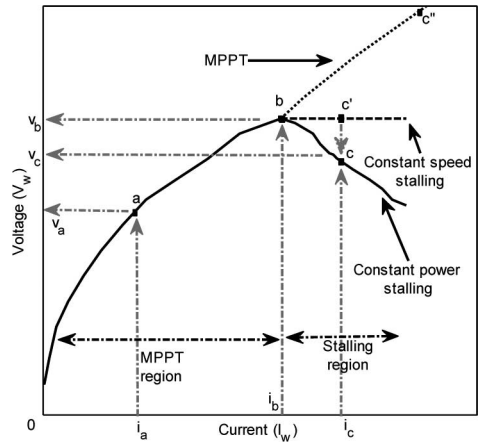

Fig. 4. DC-side voltage–current relationship.

and current as in the conventional power tracking control, there is no need to explicitly find the operating point of constant power stalling, which changes with the wind velocity. The stability and dynamic performance relies on the controller design, which is described in the next section.

Operation in the MPPT region can be shown to be inherently stable in the steady-state stability sense, while operation in the stall region needs to be stabilized using additional control terms as to be shown later. The resultant dynamic system is nonlinear and a few methods could be employed to deal with the control problem, including sliding mode [21], [22], adaptive [23], [24], and predictive control [25], or their combinations. Such methods may not be easy to implement using a simple microcontroller and may be difficult to tune. The method proposed in this study is based on designing a proportional-integral (PI) controller to regulate the rectifier dc-side voltage via generator speed at low-wind velocities, where the control objective is MPPT. At high-wind velocities, the controller aims to stall the turbine at rated power and further compensates for stability because normal control will be unstable in this region. An advantage of the method is the ease of implementation. Furthermore, the controller tuning process to produce stable soft stalling is easier and more straightforward.

The configuration shown previously in Fig. 2 consists of a VAWT driving a PMSG. The main control action is provided by the dc–dc converter. The grid-side voltage-source inverter cannot be directly used to control the PMSG due to rapid change of the dc-side voltage with wind speed. A current-source inverter can be used [16], but this will demand reactive power and prevent the inverter from operating standalone. To further explain the control concept, we now describe the design of the controller. Simulation and experimental results will then be presented to demonstrate this.

III. System Modeling and Control Design

Referring to Fig. 3(b), the generator is controlled in the MPPT mode when the wind velocity is low, i.e., below 12 m/s. As the wind velocity is increased, the power extracted from the turbine is maintained at the rated value. The control is based on a lookup table, where the rectifier dc-side current is measured to determine the target dc link voltage, as shown in Fig. 4.

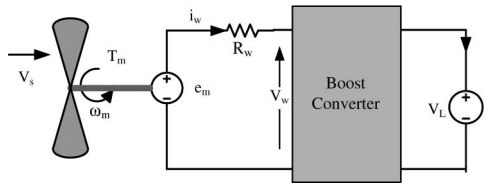

Fig. 5. Simplified wind generator system.

A. System Modeling

The electrical circuit dynamics of the generator have little effect on the overall mechanical dynamics and can be ignored in the control design. The equivalent circuit of a permanent magnet generator and the diode rectifier can be simplified, as shown in Fig. 5 viewed from the dc side of the rectifier. The Thévenin series resistance R_w has a value of twice the per phase resistance of the generator, neglecting the commutation overlap in the rectifier as the PM generator used has low inductance [12]. The source EMF (e_w) is proportional to the generator speed (ω_m)

$$e_w = K_w \omega_m \tag{1}$$

where K_w is a constant depending on the machine design.

The Thévenin equivalent of the generator and diode bridge rectifier feeds a boost type dc–dc converter, which supplies the dc link of the grid inverter represented as a voltage source v_L. The power drawn by the inverter from the dc link maintains the voltage constant; with a passive diode rectifier, the power level is to be set by the duty cycle control of the dc–dc converter. The turbine torque is represented by the following equation:

$$T_m = \frac{1}{2} \frac{\rho A R v_s^2 C_p(\lambda)}{\lambda} \tag{2}$$

taking into account that

$$\lambda = \frac{\omega_m R}{v_s}. \tag{3}$$

With a fixed pitch angle, the whole operating region of C_p can be approximated in the following quadratic form as a function of λ:

$$C_p = a_1 \lambda^2 + a_2 \lambda + a_3. \tag{4}$$

The coefficients of this equation can be obtained using curve-fitting techniques. Values of the coefficients for the turbine used here, with the power characteristic shown in Fig. 3(a), are given in the Appendix, together with other parameters of the system. Neglecting damping and friction, the mechanical dynamics can be reduced to

$$J \frac{d\omega_m}{dt} = T_m - T_e \tag{5}$$

$$T_e = \frac{P_e}{\omega_m} = \frac{e_w i_w}{\omega_m} = K_w i_w. \tag{6}$$

From (1), (5), and (6)

$$\frac{de_w}{dt} = -\frac{K_w}{J} i_w + b_1 v_s e_w + b_2 v_s^2 + b_3 \frac{v_s^3}{e_w} \tag{7}$$

where

$$b_1 = \frac{K_t R a_1}{J}$$
$$b_2 = \frac{K_t K_w a_2}{J}$$
$$b_3 = \frac{K_t K_w^2 a_3}{JR}$$
$$K_t = 0.5\rho AR.$$

On the electrical side, the relationship between the dc-side voltage of the rectifier and the voltage as the input to the grid-side inverter can be simplified as follows:

$$v_w = (1-d)v_L. \tag{8}$$

The average dc-side current can be calculated as follows:

$$i_w = \frac{1}{R_w}[e_w - (1-d)v_L]. \tag{9}$$

Linearization and combination of (7)–(9) gives the following equation, which represents the total system dynamics:

$$\frac{de_w}{dt} = A_1 e_w + B_1 d + B_2 v_L + B_3 v_s \tag{10}$$

where

$$A_1 = -\frac{K_w^2}{JR_w} + b_1 V_{s0} - \frac{b_3 V_{s0}^3}{E_{w0}^2}$$
$$B_1 = -\frac{K_w^2 V_{L0}}{JR_w}$$
$$B_2 = \frac{K_w^2 (1-D_0)}{JR_w}$$
$$B_3 = b_1 E_{w0} + 2b_2 V_{s0} + \frac{3b_3 V_{s0}^2}{E_{w0}}.$$

Based on the dynamic model, a controller as shown in Fig. 6 can be designed. The control objective is to force the turbine to a specific speed according to the measured dc-side current by means of power control, as implied by Fig. 4. The encoderless speed control is implemented by controlling the average dc-side voltage at the rectifier output. $v_w = f(i_w)$ is a lookup table relating the dc-side current and the reference dc-side voltage. The transfer function of the PI controller in the speed loop is defined as follows:

$$C(s) = \frac{K_p s + K_i}{s} \tag{11}$$

where gains K_p and K_i are determined based on the linearized system model at the rated wind velocity. Ziegler–Nichols tuning algorithm, built in the MATLAB Control System Toolbox, was used to determine the values for the test system: $K_p = -0.38$ and $K_i = -0.11$. Empirically, this would give a satisfactory step response of the model.

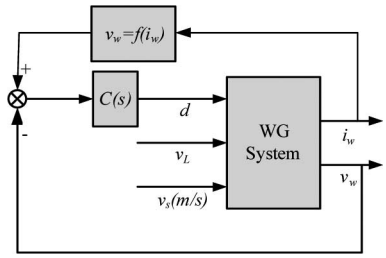

Fig. 6. PI control algorithm.

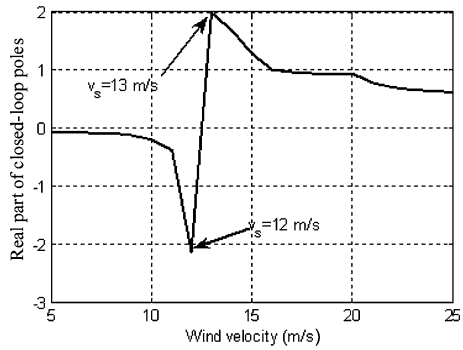

Fig. 7. Stability analysis of original control algorithm.

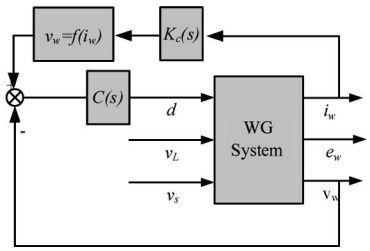

Fig. 8. Control algorithm with stability compensation.

Fig. 7 shows how the real part of the poles of the closed-loop system changes as the wind velocity increases. The poles are obtained using the closed-loop transfer function, which can be derived from the earlier relationships. Below 12 m/s, the real part is negative. It becomes positive and the system is unstable when the wind velocity is above 12 m/s. This is true for all values of K_p and K_i due to the operation in the stall region.

B. High-Wind Velocity Stability Compensation

To compensate for stability in the stall region, a pole is added in the dc-side current feedback loop, as shown in Fig. 8, where

$$K_c(s) = \frac{1}{T_c s + 1}. \tag{12}$$

This first-order lag will not change the steady-state condition, but will make the desired speed change more slowly. It tends to stabilize the equilibrium point in the stall region because the effect of variation in i_w is attenuated giving the PI controller time to keep the turbine/generator speed constant until the disturbance is over. The value of T_c is thus chosen according to the moment of inertia (J). To demonstrate this, the transfer function

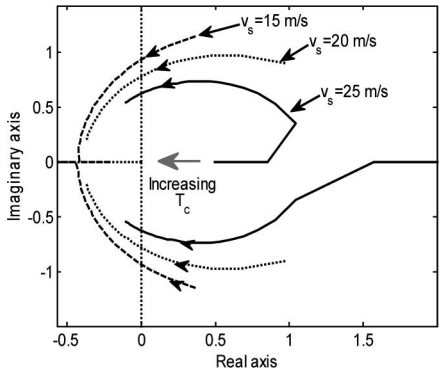

Fig. 9. Root locus of closed-loop system.

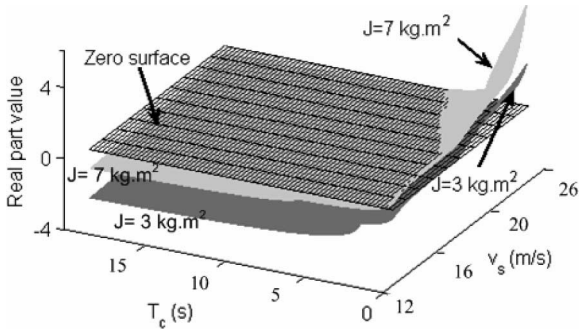

Fig. 10. Effect of inertia on the value of T_c to stabilize the system.

from the wind velocity (V_s) to the produced EMF (E_w), which is directly proportional to the rotor speed, is derived from (10)–(12) as follows:

$$E_w = \frac{B_3(s^2 + d_1 s + d_2)}{s^3 + n_1 s^2 + n_2 s + n_3} V_s \tag{13}$$

where

$$d_1 = \frac{1 - K_p V_{L0} - T_c K_i V_{L0} - K_{VI} K_p V_{L0}/R_w}{T_c(1 - K_p V_{L0})}$$

$$d_2 = \frac{-K_i V_{L0} - K_{VI} K_i V_{L0}/R_w}{T_c(1 - K_p V_{L0})}$$

$$n_1 = d_1 - A_1$$

$$n_2 = d_2 - \frac{B_1 K_{VI} K_p}{R_w T_c(1 - V_{L0} K_p)} - d_1 A_1$$

$$n_3 = -\frac{B_1 K_{VI} K_i}{R_w T_c(1 - V_{L0} K_p)} - d_2 A_1$$

$$K_{VI} = 2m_1 I_{w0} + m_2$$

where m_1 and m_2 are the coefficients of a quadratic curve-fitting function for the entire *V–I* characteristics shown in Fig. 4, which are used in the control design. It is noted that the designed controller can be further tuned on a computer model using a more accurate representation (e.g., a lookup table) of the desired *V–I* relationship

$$V_w = m_1 I_w^2 + m_2 I_w + m_3. \tag{14}$$

Fig. 9 shows the loci of the dominant roots of the closed-loop system against time constant T_c. Without the first-order lag, the system is unstable as soon as the increased wind velocity activates the stalling operating mode. As T_c increases, the real part of the roots move toward the left-hand side of the complex plane and the system is stabilized.

Targeting a maximum wind velocity of 25 m/s, it is found that for the test system, the minimum value of T_c (in seconds) is about the same as the moment of inertia *J* (in kg·m^2). This is incidental and depends on the maximum wind velocity chosen. To show the effect of moment of inertia (*J*) on the stabilizing T_c value, Fig. 10 plots the change of the real part of the dominant pole with wind velocity and T_c for two different values of (*J*). The figure demonstrates that as the inertia increases the system will be stable at a higher value of T_c. It is found that choosing T_c slightly greater than the value of the inertia (*J*) is sufficient to stabilize the system with an acceptable margin.

The aerodynamic characteristic of a VAWT relies on many factors, including the solidity. Higher solidity means that the $C_p - \lambda$ curve will have a narrower range of λ, and the maximum C_p will occur at a lower λ [26]. The turbine in this study has a medium solidity, self-starting torque, and rigid design; the tip speed ratio values seen in Fig. 3(a) are on the low side compared to some other turbines. The solidity will also affect the moment of inertia, which has been shown to be important in the controller design. It is noted that the thrust force on the rotor generally reduces as the turbine is sent into the stall region [27]. While it is expected that the concept of constant power soft stalling can be applied to many different types of VAWT, customized design of the controller will be necessary to recognize the characteristics of individual turbine series. It is hoped that this study provides a useful guideline for such an exercise.

C. Adaptive Soft-Stalling Control Loop

A method has been proposed to compensate for the stability of the system operating in the stall mode by adding a pole (first-order lag) in the current feedback loop, as shown earlier in Fig. 8. This is only needed at excessive wind velocities. At low-wind velocities, the system is inherently stable and using it will result in sluggish response reducing the MPPT efficiency.

To delay feedback at high-wind velocities and to avoid MPPT efficiency reduction, an adaptive time constant (T_c) is proposed. The time constant value needs to be high at high-wind velocities and to be zero at low-wind velocities, therefore, T_c is calculated online as a function of the average dc-side current of the diode rectifier

$$K_c(s) = \frac{1}{T_c(i_w)s + 1}. \tag{15}$$

The effect of using such an adaptive feedback is demonstrated by simulation in Fig. 11 for the test system, where a step change of wind velocity (from 0 to 12 m/s) is applied at $t = 15$ s. The output power response shows faster tracking capability using the adaptive delay control loop ($T_c = 0$) as compared to a fixed time constant ($T_c = J$) needed to stabilize the system at the highest wind velocity. The difference shows the benefit of an adaptive scheme.

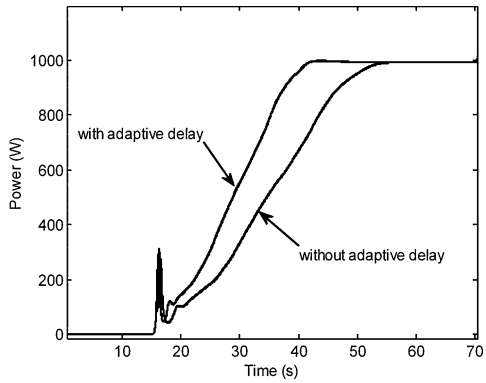

Fig. 11. Adaptive control loop effect.

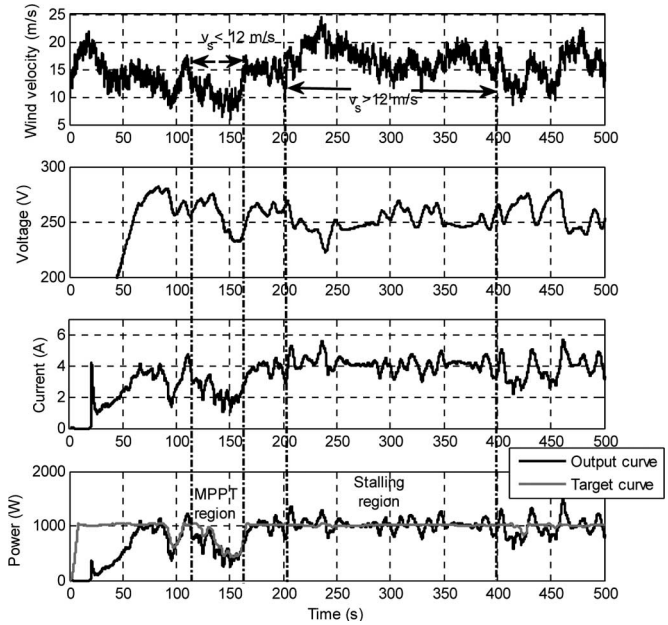

Fig. 12. Simulation results with turbulent wind changes.

IV. Simulation Results

The system simulated is grid connected, as shown in Fig. 2, and has an S1210 H-type Darrieus VAWT driving a PMSG. The PMSG supplies power to the grid through the power electronics interface stage as described in this paper. The boost converter acts as the wind generator controller. The $C_p - \lambda$ curve of the turbine is the same, as shown previously in Fig. 3(a). A set of simulation results is presented in Fig. 12, showing the wind velocity, diode rectifier dc-side voltage, dc-side current, and the output power. The target power is also shown for the wind turbine generator in gray line according to the same wind profile. The wind velocity changes between 6 and 24 m/s.

Focus first on the period between $t = 120$ and 160 s. The controller works in the MPPT mode because the wind velocity is below 12 m/s and the output power is correspondingly less than the rated value (1000 W). Then, consider the period from $t = 200$ to 400 s when the wind velocity is consistently above 12 m/s. The dc-side voltage of the diode rectifier is minimum at $t = 240$ s, and this occurs when the wind velocity is at the maximum of about 24 m/s. The power during this period is controlled almost constant at the rated value, showing that the system is indeed operating in the soft-stall mode. The output power from the generator tracks the target power in all the regions.

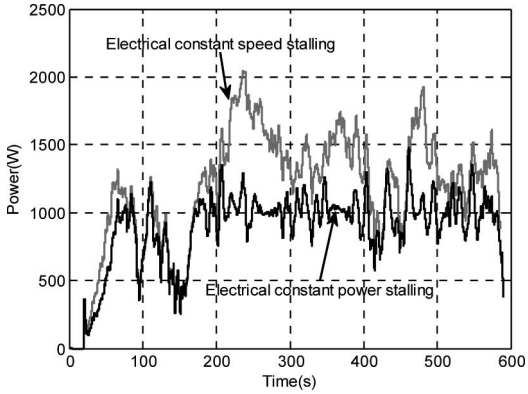

Fig. 13. Power output: constant power stalling versus constant speed stalling.

The largest power increase occurs around $t = 460$ s, caused by a fast increase of wind velocity from 13 to 18.5 m/s in less than 1 s. The turbulence is faster than the wind generator system's rotor dynamics. As a result, the control response is delayed and the power temporarily exceeds the nominal 1000 W, which should be taken into account in semiconductor device rating, but has little effect on the cooling design. As to be confirmed later by the test results, such power spikes are inevitable when the wind velocity during a gust quickly increases beyond its rated value. However, the amplitude of the resulting power "spike" is significantly lower than the power level that would result if the proposed control method were not used. This is illustrated next.

To compare constant power stalling with constant speed soft stalling, both strategies are applied to the same system, with the same wind data. The power response is contrasted in Fig. 13. The output in constant power soft stalling is lower than that in constant speed stalling at wind velocities above rated. The figure also shows that constant power stalling does not affect MPPT because with wind velocity below 12 m/s, the power is the same in both cases except in the initialization stage of the simulation. However, in the high-wind velocity range, the response in constant speed stalling reaches 2050 W, while that in constant power stalling just fluctuates around the rated power and only temporarily reaches 1500 W. Therefore, the electrical system needs to be overrated for constant speed stalling to withstand the large power at high-wind velocities, and this will increase the size and cost of the system, including the cooling design for the power semiconductor devices, which have relatively short thermal time constants. The problem is largely attenuated in constant power stalling.

V. Experimental Verification

The active soft-stalling concept at excessive wind velocities as developed in this study can prevent complex aerodynamic control and also smooth the power supplied to the grid. To verify the control method, a laboratory test is carried out and

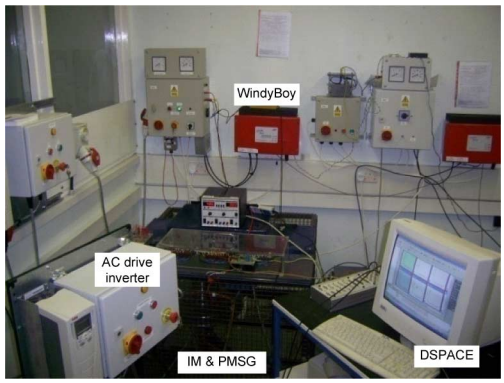

Fig. 14. Laboratory test rig.

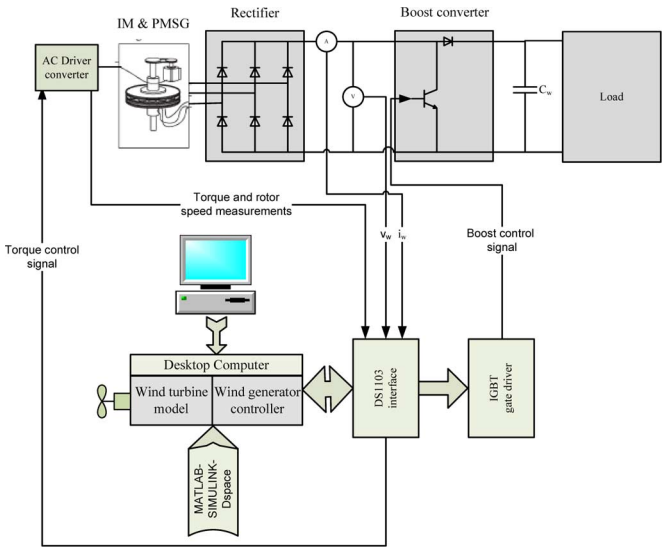

Fig. 15. Arrangement of laboratory system.

Fig. 14 shows a picture of the test rig setup. A simplified block diagram (see Fig. 15) outlines the hardware arrangement.

The VAWT itself is emulated by an induction motor (IM) driving a PMSG through a step-down gearbox. The IM is driven by an inverter working in the torque control mode, where the torque demand is set according to the measured rotational speed and the given wind velocity. The same turbine characteristic of the 1000 W system, as shown previously in Fig. 3, is implemented using a desktop computer hosting a dSPACE real-time control system, which can be programmed in the MATLAB/Simulink environment [28]. The system parameters and the control gains are the same as those used in simulation. The generated power is returned to the grid through a commercially available WindyBoy inverter ("load" in Fig. 15) set to regulate its dc link voltage.

To demonstrate the stalling control algorithm and verify the controller design, step changes of wind velocity are applied to the wind turbine system, as shown in Fig. 16. In the stall region, the wind velocity is increased up to 25 m/s. The controller stalls the generator by reducing the rectifier dc-side voltage, which is achieved by reducing the rotational speed. The power extracted from the generator is quickly regulated to be constant as the dc-side current and torque (not directly measured) increase.

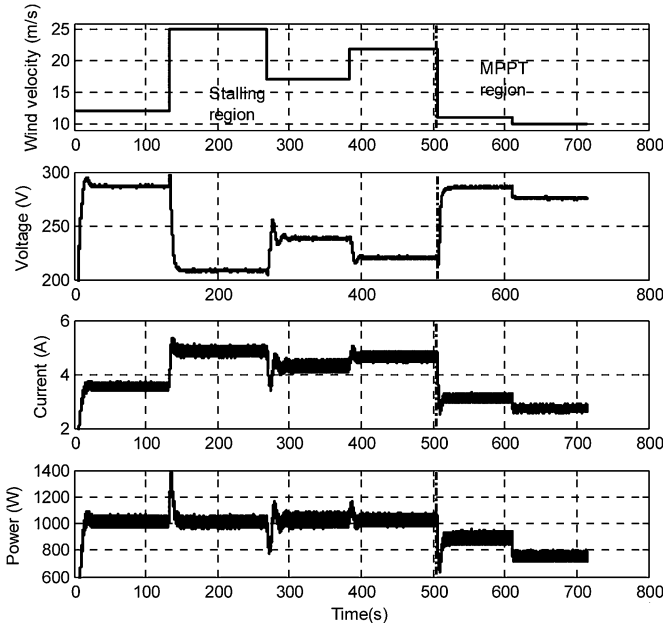

Fig. 16. Experimental results with step changes in wind velocity.

The results show that the power indeed stays roughly constant whatever the change of wind velocity is as long as it is higher than the preset 12 m/s. As the wind velocity reduces to below 12 m/s, i.e., in the MPPT region, the controller tracks the maximum power points and the power output is less than the rated 1000 W. The power increases temporarily when activating the constant power-stalling mode, depending on the difference between the initial and final values of the wind velocity. The results show that the biggest power spike happens when the maximum step change in wind velocity occurs from 12 to 25 m/s. Further examination of the results showed that the power spike at each step is less than what is predicted by simulation (not shown). This is due to the actual moment of inertia of the generator system being slightly less than the theoretical value and that there is a delay when a torque change is applied to the PMSG, which is attributed to the damper on the shaft connecting the drive to the generator.

A time-series of dynamic wind velocity similar to that used in the simulation (see Fig. 12) is used in the experiment to further demonstrate the effectiveness of the proposed control method. The experimental results are shown in Fig. 17. At $t = 30$ s, the wind velocity increases above 12 m/s. Therefore, the controller reduces the rectifier dc-side voltage by driving the system into the stall region. The dc-side current increases and the power is almost constant around 1000 W even with wind velocity being over 20 m/s. As the wind velocity returns below 12 m/s at around $t = 280$ s, the system resumes the MPPT control mode and the generated power is less than 1000 W.

The power response contains spikes with the largest occurring at about $t = 320$ s and this is because at this time the wind velocity increases at a high rate. Another observation is that the power spike at $t = 320$ s with wind velocity of 17 m/s is higher than that at $t = 410$ s with wind velocity of 23 m/s, implying

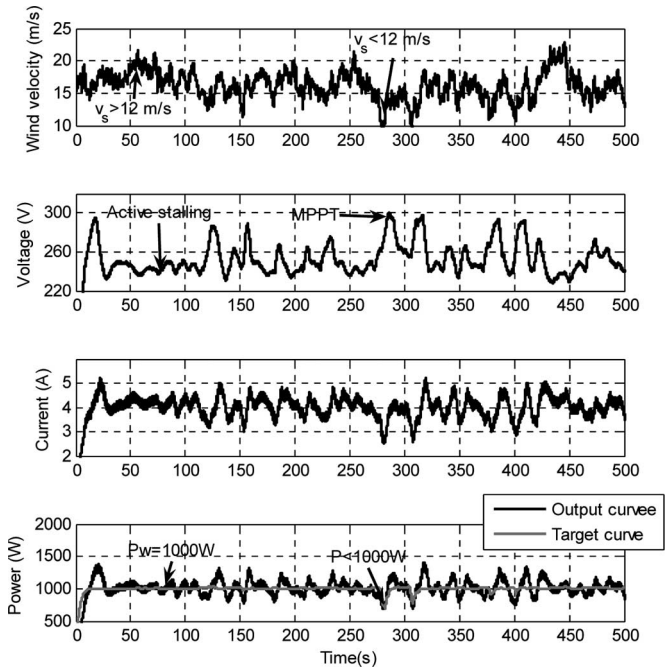

Fig. 17. Experimental results with a dynamic wind velocity time series.

that the power spike depends on the rate of change of the wind velocity.

VI. Conclusion

An electrical control scheme to deal with excessive wind velocities has been proposed for small-scale VAWTs, based on the concept of constant power soft stalling, and aims to keep the electrical power and generator speed within limits. The method is the reverse of what is normally used for MPPT control and completely avoids the need of explicitly finding the target operating point, which changes with wind velocity. The system is modeled and a PI controller is designed. As the wind velocity increases beyond the rated value, the system automatically enters the stall mode. A compensating first-order lag is added in the control loop to stabilize the system. It is found that the time constant needed increases with the turbine moment of inertia and the targeted maximum wind velocity. With different turbine characteristics and application scenarios, a customized design procedure can be carried out to determine the PI control gains and the first-order lag time constant. To prevent reduction in MPPT efficiency, the time constant can be online adapted according to the current measured on the dc side of the generator rectifier. The proposed control method has been tested by simulation and laboratory experiment.

Advantages of the proposed scheme, include simplicity of controller design, ease of implementation, avoidance for an anemometer or shaft encoder, no need for aerodynamic control, and much reduced short term overloading requirement on the generator, and power semiconductor devices. The scheme can potentially reduce the cost and size of the wind turbine generator system.

Appendix

TABLE I
PMSG and Wind Turbine Parameters

parameters	values
Wind turbine rated wind speed	12 m/s
System output power, rated value	1 kW
Generator rated current	3.4 A
Turbine radius	1 m
Generator rated voltage	240 V
Generator inductance	1.7 mH
Generator resistance	2.1 Ω
Generator emf constant	10.48 V/(rad/s)
a_1	.037
a_2	.011
a_3	-.0035
V_{L0}	400 V
Moment of inertia	5 kg.m^2

References

[1] American Wind Energy Association (AWEA). *AWEA Small Wind Turbine Global Market Study.* (2009). [Online]. Available: http://www.awea.org/

[2] British Wind Energy Association (BWEA). *BWEA Small Wind Systems U.K. Market Report 2008.* (2008). [Online]. Available: http://www.bwea.com/

[3] A. Mirecki, X. Roboam, and F. Richardeau, "Architecture complexity and energy efficiency of small wind turbines," *IEEE Trans. Ind. Electron.*, vol. 54, no. 1, pp. 660–670, Feb. 2007.

[4] W. Hu, Y. Wang, X. Song, and Z. Wang, "Development of vertical-axis wind turbine with asynchronous generator interconnected to the electric network," in *Proc. 11th Int. Conf. Electr. Mach. Syst. (ICEMS)*, Wuhan, China, Oct. 2008, vol. 1–8, pp. 2289–2293.

[5] A. Westlake, J. R. Bumby, and E. Spooner, "Damping the power angle oscillations of a permanent magnet synchronous generator with particular reference to wind turbine applications," *Inst. Electr. Eng. Proc. Electr. Power Appl.*, vol. 143, no. 3, pp. 269–280, Mar. 1996.

[6] E. Muljadi and C. P. Butterfield, "Pitch-controlled variable-speed wind turbine generation," *IEEE Trans. Ind. Appl.*, vol. 37, no. 1, pp. 240–246, Jan./Feb. 2001.

[7] Z. Chen, J. M. Guerrero, and F. Blaabjerg, "A review of the state of the art of power electronics for wind turbines," *IEEE Trans. Power Electron.*, vol. 24, no. 8, pp. 1859–1875, Aug. 2009.

[8] T. K. Barlas and G. A. M. van Kuik. (2007). "State of the art and prospectives of smart rotor control for wind turbines," *J. Phys.* [Online]. *(75)*. Available: http://www.iop.org/EJ/article/1742–6596/75/1/012080/jpconf7_75_012080.pdf

[9] A. Miller, E. Muljadi, and D. S. Zinger, "A variable speed wind turbine power control," *IEEE Trans. Energy Convers.*, vol. 12, no. 2, pp. 181–187, Jun. 1997.

[10] A. Haniotis, K. Soutis, A. Kladas, and J. Tegopoulo, "Grid connected variable speed wind turbine modeling, dynamic performance and control," in *Proc. IEEE Power Syst. Conf. Expo. (PES)*, New York, Oct. 2004, pp. 759–764.

[11] A. Ahmed, L. Ran, and J. R. Bumby, "Simulation and control of a hybrid PV-wind system," in *Proc. 4th IET Int. Conf. Power Electron., Mach. Drives*, York, U.K., Apr. 2008, pp. 421–425.

[12] J. R. Bumby, N. Stannard, J. Dominy, and N. McLeod, "A Permanent magnet generator for small scale wind and water turbines," in *Proc. 18th Int. Conf. Electr. Mach.*, Vilamoura, Portugal, Sep. 2008, pp. 1–6.

[13] E. Koutroulis and K. Kalaitzakis, "Design of a maximum power tracking system for wind-energy-conversion applications," *IEEE Trans. Ind. Electron.*, vol. 53, no. 2, pp. 486–494, Apr. 2006.

[14] M. ElMokadem, V. Courtecuisse, C. Saudemont, B. Robyns, and J. Deuse, "Fuzzy logic supervisor-based primary frequency control experiments of a variable-speed wind generator," *IEEE Trans. Power Syst.*, vol. 24, no. 1, pp. 407–417, Feb. 2009.

[15] P. P. Acarnley and J. F. Watson, "Review of position-sensorless operation of brushless permanent-magnet machines," *IEEE Trans. Ind. Electron.*, vol. 53, no. 2, pp. 352–362, Apr. 2006.
[16] K. Tan and S. Islam, "Optimum control strategies in energy conversion of PMSG wind turbine system without mechanical sensors," *IEEE Trans. Energy Convers.*, vol. 19, no. 2, pp. 392–399, Jun. 2004.
[17] H. Li, K. Shi, and P. McLaren, "Neural-network-based wind energy capture with compensated power coefficient," *IEEE Trans. Ind. Appl.*, vol. 41, no. 6, pp. 1548–1556, Nov./Dec. 2005.
[18] W. Qiao, W. Aller, and J. Harley, "Wind speed estimation based sensorless output maximization control for a wind turbine driving a DFIG," *IEEE Trans. Power Electron.*, vol. 23, no. 3, pp. 1156–1169, May 2008.
[19] S. Morimoto, H. Nakayama, M. Sanada, and Y. Takeda, "Sensorless output maximization control for variable-speed wind generation system using pmsg," *IEEE Trans. Ind. Appl.*, vol. 41, no. 1, pp. 60–67, Jan./Feb. 2005.
[20] A. Haniotis, S. Papathanassiou, A. Kladas, and M. Papadopoulus, "Control issues of a permanent magnet generator variable-speed wind turbine," *Wind Eng.*, vol. 26, no. 6, pp. 371–381, Nov. 2002.
[21] J. Hui and A. Bakhshai, "A new adaptive control algorithm for maximum power point tracking for wind energy conversion systems," in *Proc. IEEE Power Electron. Spec. Conf.*, Jun. 2008, vol. 1–10, pp. 4003–4007.
[22] F. Valenciaga and P. F. Puleston, "High-order sliding control for wind energy conversion system based on a permanent magnet synchronous generator," *IEEE Trans. Energy Convers.*, vol. 23, no. 3, pp. 860–867, Sep. 2008.
[23] B. Beltran, M. E. Benbouzid, and T. A. Ali, "Sliding mode power control of variable-speed wind energy conversion systems," *IEEE Trans. Energy Convers.*, vol. 23, no. 2, pp. 551–558, Jun. 2008.
[24] J. M. Mauricio and A. Gomez, "An adaptive nonlinear controller for DFIM-based wind energy conversion systems," *IEEE Trans. Energy Convers.*, vol. 23, no. 4, pp. 1025–1035, Dec. 2008.
[25] R. Cárdenas and R. Peña, "Sensorless vector control of induction machines for variable-speed wind energy applications," *IEEE Trans. Energy Convers.*, vol. 19, no. 1, pp. 196–205, Mar. 2004.
[26] B. Kirke, "Evaluation of self-starting vertical-axis wind turbines for stand-alone applications," Ph.D. thesis, Griffith Univ., Australia, 1998.
[27] T. Burton, D. Sharpe, N. Jenkins, and E. Bossanyi, *Wind Energy Handbook*. Sussex, England: Wiley, 2001, pp. 173–177.
[28] dSPACE. (2006, Oct. 18) "DS1103 PPC controller board," [Online]. Available: http://www.dspace.ltd.uk/ww/en/ltd/home/products/hw/singbord/ppcconbo.cfm

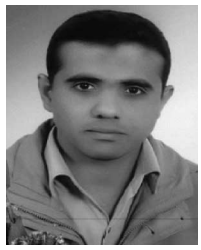

Ashraf Ahmed (S'09) received the B.Sc. degree from Assiut University, Assiut, Egypt, in 1999, and the M.Sc. degree from Cairo University, Cairo, Egypt, in 2005, both in electrical engineering. He is currently working toward the Ph.D. degree in renewable energy system control and power electronics from Durham University, Durham, U.K.

Since 2001, he has been a Research Assistant in the Desert Research Institute, Cairo, Egypt.

Li Ran (M'98–SM'07) received the Ph.D. degree in power systems engineering from Chongqing University, Chongqing, China, in 1989.

He is currently a Reader in electrical power and control in the School of Engineering and Computing Sciences, Durham University, Durham, U.K. His research interests include the application of power electronics in power systems and renewable energy systems, such as wave and wind energy converters.

Jim R. Bumby received the M.Eng. and Ph.D. degrees in engineering from the University of Durham, Durham, U.K., in 1970 and 1974, respectively.

He is currently a Reader in electrical engineering in the School of Engineering and Computing Sciences, Durham University, Durham, U.K. His research interests include electrical power and control, and novel generator topologies for new and renewable energy systems.